X-ray Structure of the Magnesium(II)·ADP·Vanadate Complex of the *Dictyostelium discoideum* Myosin Motor Domain to 1.9 Å Resolution[†,‡]

Clyde A. Smith[§] and Ivan Rayment*

Institute for Enzyme Research and Department of Biochemistry, University of Wisconsin, Madison, Wisconsin 53705

Received November 6, 1995; Revised Manuscript Received January 30, 1996[⊗]

ABSTRACT: The structure of the vanadate-trapped ADP complex of a truncated head of *Dictyostelium* myosin II consisting of residues Asp 2−Asn 762 has been determined by molecular replacement at 1.9 Å resolution and refined to a crystallographic *R*-factor of 19.4%. The crystals belong to the orthorhombic space group $C222_1$ where $a = 84.50$ Å, $b = 145.4$ Å, and $c = 152.8$ Å. The conformation of the protein is similar to that of MgADP·AlF_4·S1Dc [Fisher, A. J., et al. (1995) *Biochemistry 34,* 8960−8972]. The nucleotide binding site contains a complex between MgADP and vanadate where MgADP exhibits a very similar conformation to that seen in previous complexes. The vanadate ion adopts a trigonal bipyramidal coordination. The three equatorial oxygen ligands are fairly short, average 1.7 Å, relative to a single bond distance of ∼1.8 Å and are coordinated to the magnesium ion, Nζ of Lys 185, and five other protein ligands. The apical coordination to the vanadate ion is filled by a terminal oxygen on the β-phosphate of ADP and a water molecule at bond distances of 2.1 and 2.3 Å, respectively. The long length of the apical bonds suggests that the bond order is considerably less than unity. This structure confirms the earlier suggestion that vanadate is a model for the transition state of ATP hydrolysis and thus provides insight into those factors that are responsible for catalysis. In particular, it shows that the protein ligands and water structure surrounding the γ-phosphate pocket are oriented to stabilize a water molecule in an appropriate position for in-line nucleophilic attack on the γ-phosphorus of ATP. This structure reveals also an orientation of the COOH-terminal region beyond Thr 688 which is very different from that observed in either MgADP·BeF_x·S1Dc or chicken skeletal myosin subfragment 1. This is consistent with the COOH-terminal region of the molecule playing an important role in the transduction of chemical energy of hydrolysis of ATP into mechanical movement.

The orthovanadate ion is a potent inhibitor of many enzymes that catalyze phosphoryl transfer (Gresser & Tracey, 1990). It is an effective inhibitor in part because it has very similar size and charge to inorganic phosphate but also because it readily increases its coordination sphere to five and exhibits considerable plasticity in its bond distances (Holloway & Melnick, 1986). These features allow this ion to adopt a trigonal bipyramidal coordination that has been proposed to mimic the conformation of the phosphate group at the transition state expected for phosphoryl transfer (Lindquist et al., 1973; Westheimer, 1987) and has been observed in the complex of ribonuclease with uridine vanadate (Wlodawer et al., 1983). As a consequence of these properties vanadate has proved to be a valuable tool for studying enzyme mechanism. This is particularly true for myosin, the major ATPase of muscle, that is inhibited strongly by vanadate both in solution and in muscle fibers (Goodno, 1979; Dantzig & Goldman, 1985).

In myosin, ATP hydrolysis is not coincident with the force-generating step (Lymn & Taylor, 1971; Goldman, 1987). Instead, ATP binding initially reduces the affinity of myosin for actin, after which hydrolysis of ATP occurs rapidly and results in a metastable ternary complex between myosin, ADP, and inorganic phosphate. In this state the equilibrium complex between ATP and ADP,P_i is between 1 and 10 for skeletal muscle depending on the temperature and ionic strength (Bagshaw & Trentham, 1973, 1974; Taylor, 1977). Release of the hydrolysis products is catalyzed by rebinding to actin which is accompanied by the energy transduction step. Vanadate inhibits the myosin ATPase activity by forming, in the absence of actin, a long-lived complex with MgADP that is believed to mimic either the transition state for hydrolysis or the ADP,P_i state (Goodno, 1979; Goodno & Taylor, 1982). The half-life for dissociation of this complex at 0 °C is ∼4 days (Goodno, 1979, 1982; Werber et al., 1992). Interestingly, the rate of inhibition is considerably less than the diffusion limit for binding. Thus, formation of the inhibitory ternary complex was interpreted as a multistep process, in which there was initial formation of an equilibrium complex, followed by slow isomerization to form the inhibited state. Furthermore, ADP·Vi[1] reduces

[†] This research was supported in part by NIH Grant AR35186 to I.R. and Grant Tw05194 from the Fogarty International Center, NIH, to C.A.S.

[‡] The X-ray coordinates have been deposited in the Brookhaven Protein Data Bank (file name 1VOM).

* To whom correspondence should be addressed at the Institute for Enzyme Research, 1710 University Ave., Madison, WI 53705. Phone: (608) 262-0529. Fax: (608) 265-2904. E-mail: ivan@enzyme.wisc.edu.

[§] Present address: Department of Chemistry and Biochemistry, Massey University, Palmerston North, New Zealand.

[⊗] Abstract published in *Advance ACS Abstracts,* March 15, 1996.

[1] Abbreviations: myosin S1, myosin subfragment 1; S1Dc, *Dictyostelium discoideum* myosin motor domain; PMSF, phenylmethanesulfonic acid; BTP, bis-Tris-propane; MgPP$_i$·S1Dc, magnesium pyrophosphate complex of truncated *D. discoideum* myosin motor domain; EG, ethylene glycol; MgADP·BeF_x·S1Dc, the beryllium fluoride−ADP complex of *D. discoideum* myosin motor domain; MgADP·AlF_4·S1Dc, the aluminum fluoride−ADP complex of *D. discoideum* myosin motor domain; MgADP·VO_4·S1Dc, the vanadate−ADP complex of *D. discoideum* myosin head; S1, subfragment-1; Vi, vanadate (VO_4^{3-}).

S0006-2960(95)02633-X CCC: $12.00

the binding affinity of myosin for actin (1.5×10^{-3} M^{-1}), although less than that induced by the ADP,P_i state under the same conditions. Actin also increases the rate of release of vanadate by 10^5 compared to that of myosin·ADP·Vi alone, although the release of vanadate is still slow. The actin-activated ATPase activity of myosin is about 90% inhibited by ADP·Vi at high vanadate concentrations (Goodno & Taylor, 1982); however, there is some indication that this is due in part to the formation of polymeric vanadate ions (Smith & Eisenberg, 1990). Spectroscopic studies of spin-labeled myosin subfragment 1 have also shown that the ADP·Vi complex exhibits many of the structural properties of the ADP,P_i state (Wells & Bagshaw, 1984). Consequently, the ADP·Vi complex is often considered to be close to the conformation of myosin at the start of the power stroke.

Formation of the metastable, yet dynamic, ADP,P_i state is an unusual feature for an enzyme. The MgADP·Vi complex provides an opportunity to arrest the contractile cycle at a critical point and provides a chance to study this important state. A detailed study of the mechanical properties of muscle fibers revealed that tension and stiffness in actively contracting fibers are suppressed by vanadate and that this is due to the formation of a long-lived MgADP·Vi complex analogous to that observed with myosin alone (Dantzig & Goldman, 1985). This allowed the role of a specific state in the contractile cycle to be characterized under differing physiological conditions (Dantzig & Goldman, 1985; Chase et al., 1993; Wilson et al., 1995).

Vanadate has also proved to be a valuable tool for mapping the active site of myosin due to the stability of divalent metal ADP·Vi complexes. This stability allowed complexes of myosin with photoreactive ADP analogs to be separated from excess reagent prior to irradiation, which dramatically improved the specificity of labeling (Yount et al., 1992). As a consequence a significant number of residues in the active site were unequivocally identified. The vanadate ion itself is also photoreactive. Illumination of the myosin·ADP·Vi complex with UV light above 300 nm causes modification of a specific serine in the active site of skeletal muscle myosin and release of vanadate (Cremo et al., 1988, 1989; Grammer et al., 1988). Subsequent rebinding of MgADP·Vi and further illumination results in peptide bond cleavage, as in other systems (Gibbons et al., 1987; Grammer et al., 1988). These reactions served to identify a critically important serine residue in the coordination of the γ-phosphate. Together, these chemical studies played an important role in the development of a structural mechanism for the myosin ATPase activity (Rayment et al., 1993a,b; Fisher et al., 1995a,b).

It is thus evident that considerable biochemical and biophysical effort has been expended on the MgADP·Vi complex of myosin as part of the greater goal of understanding the molecular basis of muscle contraction. We report here the structure of the MgADP·VO_4 complex of the truncated head of *Dictyostelium discoideum* at 1.9 Å resolution. This study complements earlier structures of the truncated myosin head of *Dictyostelium* myosin complexed with MgADP·BeF_x[2] and MgADP·AlF_4^- which mimic the ATP and transition-state states, respectively (Fisher et al., 1995a,b). The vanadate complex represents a more realistic analog of the transition state than the structure of MgADP·AlF_4·S1Dc that was reported only at 2.6 Å resolution. As such, it indicates the structural features that are important for catalysis. Furthermore, the present model reveals the orientation of the COOH-terminal domain and the loops that connect the major tryptic fragments which were missing in the structure of MgADP·AlF_4·S1Dc.

EXPERIMENTAL PROCEDURES

Protein Purification and Crystallization. Truncated myosin subfragment 1, residues Asp 2 to Asn 762, from *D. discoideum* (S1Dc) was purified as described previously (Fisher et al., 1995b). Prior to crystallization, MgADP was trapped in the active site by the addition of stock solutions to a final concentration of 2 mM ADP, 3 mM sodium vanadate, and 1 mM $MgCl_2$. A stock solution of 400 mM vanadate at pH 10.0 was prepared as described by Goodno (1982). Crystals of the vanadate-trapped ADP complex of myosin S1 (MgADP·VO_4·S1Dc) were grown by microbatch from 8.5% PEG 8000, 25 mM Hepes, pH 7.0, 250 mM NaCl, 2 mM DTT, and 3% 2-methyl-2,4-pentanediol. The protein concentration in the final droplet was about 5 mg/mL. The protein/precipitant solutions were microseeded from preliminary hanging-drop experiments and left at 4 °C. Small crystals generally appeared overnight and typically took from 2 to 3 weeks to reach maximum dimensions of $0.6 \times 0.4 \times 0.15$ mm.

Data Collection and Processing. The MgADP·VO_4·S1Dc crystals are orthorhombic with unit cell dimensions $a = 88.5$ Å, $b = 145.4$ Å, and $c = 152.8$ Å and belong to space group $C222_1$. The crystals are isomorphous with those of the aluminum fluoride-trapped ADP complex of myosin S1, MgADP·AlF_4·S1Dc, which has cell dimensions of $a = 87.9$ Å, $b = 149.0$ Å, and $c = 153.8$ Å (Fisher et al., 1995b). High-resolution X-ray data were collected with a MAR detector from one frozen crystal on beamline 7-1 at the Stanford Synchrotron Radiation Laboratory. The crystal was transferred from the crystallization medium into a synthetic mother liquor containing 15% PEG 8000, 300 mM NaCl, 2 mM ADP, 3 mM sodium vanadate, 1 mM $MgCl_2$, and 5% ethylene glycol (EG) in 25 mM Hepes, pH 7.0, for transportation. Prior to freezing, the crystal was transferred gradually into a solution containing 18% PEG 8000, 300 mM NaCl, 2 mM ADP, 3 mM sodium vanadate, 1 mM $MgCl_2$, 30% EG, and 25 mM Hepes, pH 7.0. The crystal was placed into three solutions consisting of 1:3, 2:2, and 3:1 18% PEG buffered as above:cryoprotectant mother liquor, 5 min per step, and then finally into the cryoprotectant mother liquor for a final 5 min. A droplet of this solution containing the crystal was picked up in a loop of surgical suture and rapidly frozen in a stream of nitrogen at −160 °C (Teng, 1990; Rodgers, 1994).

X-ray data were collected with the oscillation method (Arndt & Wonacott, 1977) on a 30 cm MAR detector at a wavelength of 1.08 Å. An oscillation range of 1° was used, and 95 frames were recorded with a crystal-to-image distance of 120 mm. The images were processed with the program DENZO (Otwinowski, 1986) and scaled and merged using ROTAVATA and AGROVATA from the CCP4 suite of programs (CCP4, 1994). Partially recorded reflections

[2] The exact composition of the beryllium fluoride species is unknown (Henry et al., 1993) whereas the aluminum fluoride complex has been shown to contain four equivalent fluorine atoms (Maruta et al., 1993). Consequently, these complexes will be designated as BeF_x and AlF_4^-.

Table 1: X-ray Data Processing

no. of crystals used	1
maximum resolution (d_{min}, Å)	1.90
total reflections measured to d_{min}	393986
independent reflections to d_{min}	75066
R_{merge} (%)[a]	2.8
theoretical no. of reflections to d_{min}	77683
cumulative % completeness	97
% completeness in highest resolution shell[b]	92
unit cell parameters	
a (Å)	88.5
b (Å)	145.4
c (Å)	152.8

[a] $R = \Sigma|I - \bar{I}|/\Sigma I \times 100$. [b] 1.97− 1.9 Å.

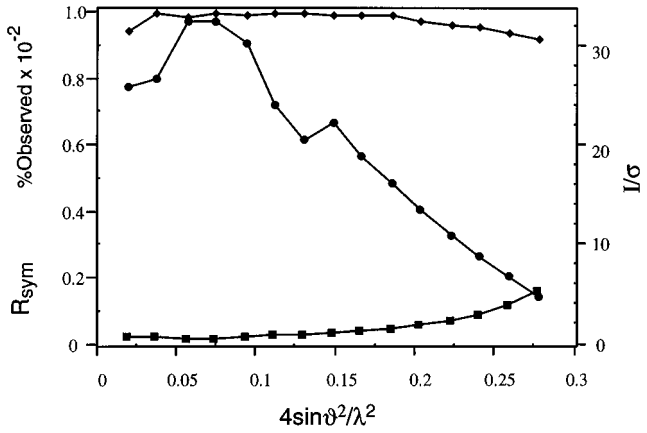

FIGURE 1: Percentage of the theoretical number of reflections (♦), the average I/σ (●) as a function of 4 $\sin^2\theta/\lambda^2$, and R_{merge} (■) as a function of 4 $\sin^2\theta/\lambda^2$ for the final MgADP·VO_4·S1Dc data set.

recorded on adjacent images were added to give full reflections, while the intensities of partials with no match on adjacent images and with calculated partialities greater than 0.7 were scaled by the inverse of their partiality. Of the 393 986 measured reflections, 138 354 were fully recorded and 88 639 were partially recorded. A final unique, non-zero data set of 75 066 reflections was obtained with an R_{merge} of 0.028 on intensities ($R_{merge} = \Sigma|I - \bar{I}|/\Sigma I$). The data set was 97% complete to 1.9 Å resolution (Table 1). Figure 1 shows the variation of the completeness of the data and R_{merge} as a function of resolution. In the highest resolution shell, between 1.97 and 1.9 Å, the data are 92% complete, with an average I/σ of 4.9.

Structure Determination and Refinement. Although the MgADP·VO_4·S1Dc crystals were essentially isomorphous with those of MgADP·AlF_4·S1Dc, an initial crystallographic *R*-factor calculated between the MgADP·AlF_4·S1Dc model refined at 2.6 Å (Fisher et al., 1995b) and the MgADP·VO_4·S1Dc data was 48.5%. This was possibly due to the changes in the cell parameters between the two crystals. Consequently, the molecular replacement program AMORE (Navaza, 1993) was used to place the model of MgADP·AlF_4·S1Dc in the cell. This revealed that the there was a rotation and translation of 1° and 0.75 Å between the coordinates in these two cells.

Prior to refinement of the MgADP·AlF_4·S1Dc-derived model against the X-ray data, the solvent molecules, the Mg^{2+}·ADP, and the AlF_4^- were removed, along with 10 residues at the COOH terminus. The model consisted of 5500 protein atoms (650 residues) comprising residues Asn 2−Gln 19, Thr 28−Val 65, Gly 68−Gly 201, Ser 208−Phe 487, Asp 509−Arg 620, and Asn 626−Gly 680. The structure was refined with 20 cycles of conjugate gradient refinement with the program TNT (Tronrud et al., 1987) while increasing the resolution from 3.0 to 2.3 Å, resulting in a drop in the crystallographic *R*-factor from 0.415 to 0.343. A $2F_o - F_c$ electron density map displayed on an Evans and Sutherland PS390 with the molecular graphics program FRODO (Jones, 1978, 1985) showed continuous density for all the atoms in the initial model, along with density for some of the missing residues. In addition, electron density in the vicinity of the active site could be clearly identified as an ADP moiety. Contouring an $F_o - F_c$ electron density map at 6σ showed a peak between the side chains of Thr 186 and Ser 237, ligands of the magnesium ion in MgADP·BeF_x·S1Dc, MgADP·AlF_4·S1Dc (Fisher et al., 1995b), and $MgPP_i$·S1Dc (Smith & Rayment, 1995). An Mg^{2+} ion was built into this density together with two solvent molecules that were clearly interacting with the Mg^{2+}. The density for the vanadate group at a height of $>20\sigma$ could be seen in both maps adjacent to the β-phosphate of the ADP and connected to the Mg^{2+} density. This was not built in at this stage, since the orientation of the atoms surrounding the vanadium atom could not be unambiguously determined.

Over the course of 20 more stages of TNT refinement and manual model rebuilding, the resolution limits were extended to 20.0−1.9Å and several pieces of missing structure were added. The electron density adjacent to the ADP and Mg^{2+} ion was clearly trigonal planar in shape, with a small lobe of density perpendicular to the plane. A trigonal planar VO_3 group was added to the model with a fourth oxygen atom occupying a small lobe of density in an apical position relative to the VO_3 plane and directly opposite one of the oxygen atoms on the β-phosphate, the fifth vanadium ligand. The NH_2-terminal section of the polypeptide chain was completed. This region is folded somewhat differently from the corresponding area in MgADP·BeF_x·S1Dc, due primarily to the close contact of a symmetry-related molecule. The helix between Lys 488 and Asn 500, which could not be readily traced in the MgADP·AlF_4·S1Dc structure, was also added to the model. This helix adopts a different conformation from the corresponding helix in MgADP·BeF_x·S1Dc, in that the helix is markedly bent at Lys 488. The polypeptide chain from Asn 500 to Asp 509, missing in the three previous S1Dc structures determined to date, was located after refinement of the newly located helix between Lys 488 and Asn 500. Finally, residues Arg 620 to Asn 626, a flexible loop region at the junction between the central 50 kDa and the COOH-terminal 20 kDa sections of the heavy chain, were built into weak but continuous electron density.

The position of the helix between Gln 480 and Asn 500 led to the location of parts of the missing COOH-terminal section. Superposition of the COOH-terminal domain from MgADP·BeF_x·S1Dc, based on the position of this helix, revealed several parts of the missing domain corresponding to three strands (Lys 690−Tyr 698, Glu 735−Phe 739, and Thr 742−Arg 747) which were subsequently built into the density as polyalanine. Residues Lys 690−Glu 759 from MgADP·BeF_x·S1Dc were superimposed upon the newly located COOH terminus of MgADP·VO_4·S1Dc on the basis of these three strands, and these rotated coordinates were appended to model for MgADP·VO_4·S1Dc. Simulated annealing refinement with the program X-PLOR (Brünger et al., 1987; Brünger, 1990), followed by positional refine-

Table 2: Refinement Statistics[a]

resolution limits (Å)	20.0−1.9
initial *R*-factor[b]	41.5
final *R*-factor	19.4
no. of reflections used	73626
no. of protein atoms	5766
no. of solvent molecules	705
other molecules, ions	1 Mg^{2+}, 1 ADP, 1 VO_4^{3-}
av *B*-value, protein atoms (Å^2)	33.1
av *B*-value, solvent atoms (Å^2)	43.3
weighted rms deviations from ideality	
bond length (Å)	0.012
bond angles (deg)	2.656
planarity (trigonal) (Å)	0.004
planarity (others) (Å)	0.010
torsional angle (deg)[c]	17.320

[a] TNT refinement. [b] $R = \Sigma||F_o| - k|F_c||/\Sigma|F_o|$. [c] No restraints were placed on torsional angles during refinement.

ment with TNT, gave an *R*-factor of 0.250. This region of the structure was further improved with omit maps calculated with SIGMAA coefficients (Read, 1986) to minimize model bias.

During the refinement and model building, a close contact was observed between the sulfhydryl group of Cys 442 and the 2-fold-related side chain in an adjacent molecule. The electron density reveals that there is an intermolecular disulfide bond between these side chains. This cysteine residue is located on the same side of the molecule as the actin binding surface but is a considerable distance from the nucleotide binding site, the actin binding site, and the COOH-terminal domain, such that it is unlikely that it influences the conformation of the molecule. This linkage was also observed in MgADP·AlF_4·S1Dc but not in MgADP·BeF_x·S1Dc. It appears that the crystal packing in MgADP·VO_4·S1Dc favors the formation of this linkage, though it is unknown if dimerization is necessary for crystal growth.

A systematic search for solvent molecules was undertaken with the programs PEAKMAX and WATPEAKS (CCP4, 1994). An $F_o - F_c$ electron density map was searched for the highest peaks above 4σ, and these peaks were then tested against the atomic coordinates of the protein to see whether they fell within a specified distance of a potential hydrogen bond donor or acceptor (between 2.4 and 3.5 Å). The location and geometry of these water molecules were checked manually on a Silicon Graphics Indigo 2 with the program O (Jones et al., 1991). A total of 705 water molecules were added to the structure during the course of the refinement.

At the completion of the refinement and model building, the final *R*-factor was 0.194 for all data (73 626 reflections) between 20.0 and 1.9 Å resolution, with rms deviations from standard bond lengths and angles of 0.012 and 2.66°, respectively. Relevant refinement statistics are given in Table 2. The average error in the model was estimated from a Luzzati plot (Luzzati, 1952) (data not shown) to be between 0.175 and 0.20 Å. A Ramachandran plot (Ramakrishnan & Ramachandran, 1965) of the main chain conformational angles (Figure 2) indicates that most of the non-glycine and non-proline residues lie within or very close to the allowed regions of conformational space. A plot of the main chain temperature factors and correlation coefficients is shown in Figure 3. A representative section of electron density is shown in Figure 4.

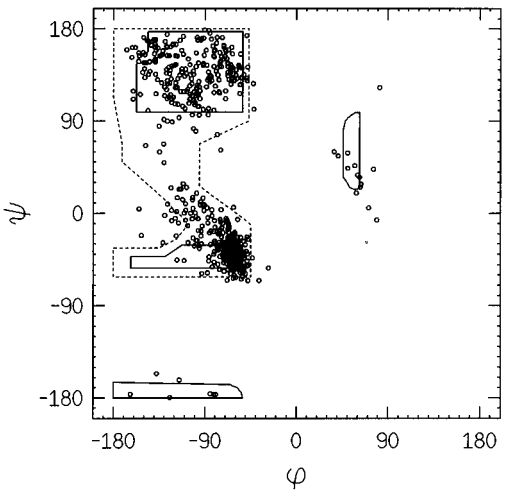

FIGURE 2: Plot of the main chain conformational torsion angles ϕ and ψ for the non-glycinyl residues in the final model for MgADP·VO_4·S1Dc.

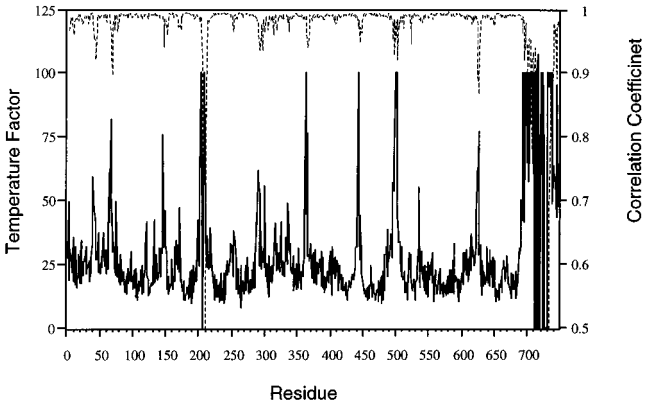

FIGURE 3: Plot of the variation of the average main chain temperature factors (solid lines) and the main chain correlation coefficients (dashed lines) with residue number. The correlation coefficients were calculated with the program OVERLAPMAP (CCP4, 1994).

RESULTS AND DISCUSSION

The Final Model. The refined MgADP·VO_4·S1Dc model consists of 5766 protein atoms, 705 solvent molecules, 1 adenosine diphosphate molecule, 1 Mg^{2+} ion, and 1 VO_4 moiety. The polypeptide chain runs from Asn 2−Gln 204, Gly 209−Pro 710, Val 712−Asp 715, Gln 720−Thr 723, and Asn 731−Arg 747. The COOH-terminal region is rather fragmented, and although three strands and parts of two helices are in the same relative orientation as the corresponding region in MgADP·BeF_x·S1Dc, there is no electron density for the loops connecting the secondary structure elements and their location cannot be identified even after superposition of the COOH terminus of MgADP·BeF_x·S1Dc onto the current model. However, the three strands all have very well-defined electron density associated with them and have good density for their side chains. This section of the MgADP·VO_4·S1Dc model is clearly not as well-defined as the remainder of the structure, as can be seen in a plot of the average main chain *B*-factor as a function of residue number (Figure 3). The average main chain *B*-value for the residues from Lys 690 to Arg 747 is 81.8 Å^2, while for the remainder of the model, the average *B*-value is 24.8 Å^2. Real space correlation coefficients (Figure 3) calculated with the

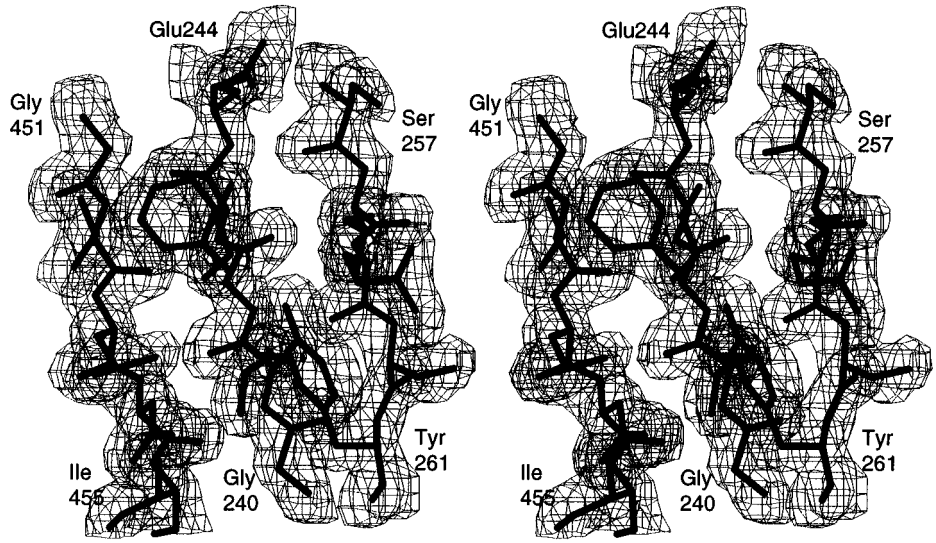

FIGURE 4: Stereoview of a piece of representative $2F_o - F_c$ electron density in the central β-sheet that forms the platform for the nucleotide binding site. This figure and Figure 8 were prepared with the programs FRODO and MOLVIEW (Jones, 1985; Smith, 1993).

program OVERLAPMAP (CCP4, 1994) also show lower than normal values for the latter part of the COOH terminus. The discussion of the structure will focus first on the overall conformation of the protein and then on the contents of the active site.

Protein Conformation. The overall conformation of residues Asn 2−Thr 688, which includes the NH_2-terminal 25 kDa, the central 50 kDa, and approximately 70 amino acid residues of the COOH-terminal 20 kDa section, is essentially identical to that of the MgADP·AlF_4·S1Dc (Fisher et al., 1995a,b). This is not unexpected since the MgADP·VO_4·S1Dc and MgADP·AlF_4·S1Dc complexes crystallize in the same space group and unit cell. The rms difference between the 643 common residues between Asn 2 and Thr 688 is 0.67 Å, where the reduction in the number of residues arises because the structure of MgADP·AlF_4·S1Dc was incomplete.

The conformation of MgADP·VO_4·S1Dc is significantly different from that of the MgADP·BeF_x·S1Dc, as was noted previously for the MgADP·AlF_4 complex (Fisher et al., 1995a,b). As before, the narrow cleft that splits the central 50 kDa section of the heavy chain is partially closed in the MgADP·VO_4 complex relative to that seen in MgADP·BeF_x·S1Dc. The conformational changes in MgADP·VO_4·S1Dc associated with Gly 457 are essentially identical to those seen in MgADP·AlF_4·S1Dc. Likewise, the hydrogen-bonding pattern at the back of the cleft is very similar even though the contents of the γ-phosphate pocket are different. However, since the MgADP·VO_4 complex was determined at higher resolution and is more complete, several sections of the molecule, including parts of the COOH-terminal domain that were previously disordered, can now be seen (Figure 5). Many of these show conformational changes relative to MgADP·BeF_x·S1Dc as discussed below.

Trp 501−Gly 507. One section missing in both MgADP·AlF_4·S1Dc and MgADP·BeF_x·S1Dc (though present in chicken skeletal S1) extends from Trp 501 to Gly 507 and contains the tryptophan residue that is believed to be responsible for the fluorescence enhancement observed during ATP hydrolysis (Hiratsuka, 1992). Tryptophan fluorescence has proved to be invaluable for following the conformational state of the myosin head during ATP hydrolysis and has provided an experimental probe for following the kinetic behavior of the contractile cycle (Morita, 1967; Werber et al., 1972; Trentham et al., 1976). This provided the evidence that ATP binding is a multistep process that consists of several distinct conformational states (Lymn & Taylor, 1971; Trybus & Taylor, 1982). It has been suggested that only one or two tryptophan residues experience an altered environment (Werber et al., 1972; Papp & Highsmith, 1993) and that these are located in the 50 kDa tryptic fragment (Werber et al., 1987). Even so, it has proved difficult to identify exactly which tryptophan(s) and hence component(s) of the protein is (are) responsible for these phenomena. It has been proposed that Trp 510 in skeletal muscle myosin (Trp 501 in S1Dc) is responsible for the fluorescence changes based on fluorescence energy transfer measurements, proximity arguments from cross-linking between SH1 and SH2 to cysteines in the 50 kDa section of the heavy chain, and sequence conservation (Warrick & Spudich, 1987; Johnson et al., 1991; Hiratsuka, 1992; Rayment et al., 1996). *Dictyostelium* myosin II exhibits a fluorescence enhancement though at a reduced level compared to that of skeletal myosin (Ritchie et al., 1993).

The section of random coil containing Trp 501 in S1Dc exhibits different conformations in the beryllium and vanadate complexes (Figure 6). Trp 501 lies under the pocket that contains the reactive cysteine residue in skeletal myosin (Thr 688 in S1Dc) and is surrounded by the hydrophobic residues Tyr 494, Phe 503, Phe 692, and a highly conserved Gly 691. These residues are conserved in chicken skeletal myosin. Trp 501 is buried in MgADP·VO_4·S1Dc whereas in chicken skeletal myosin S1 it is exposed to solvent on one edge. The exact reason for the fluorescence enhancement cannot be explained by the present structures since it is likely that the exact nature of the conformational change that occurs around Trp 501 is influenced by the essential light chain which is missing from the structures of S1Dc. It has been suggested that the fluorescence enhancement might be due to an interaction between an ionizable side chain and the indole ring (Bivin et al., 1993). The use of the ADP,Vi complex to account for the fluorescence enhancement must also be qualified by the observation that in rabbit skeletal muscle myosin the ADP,Vi complex shows a lower level of

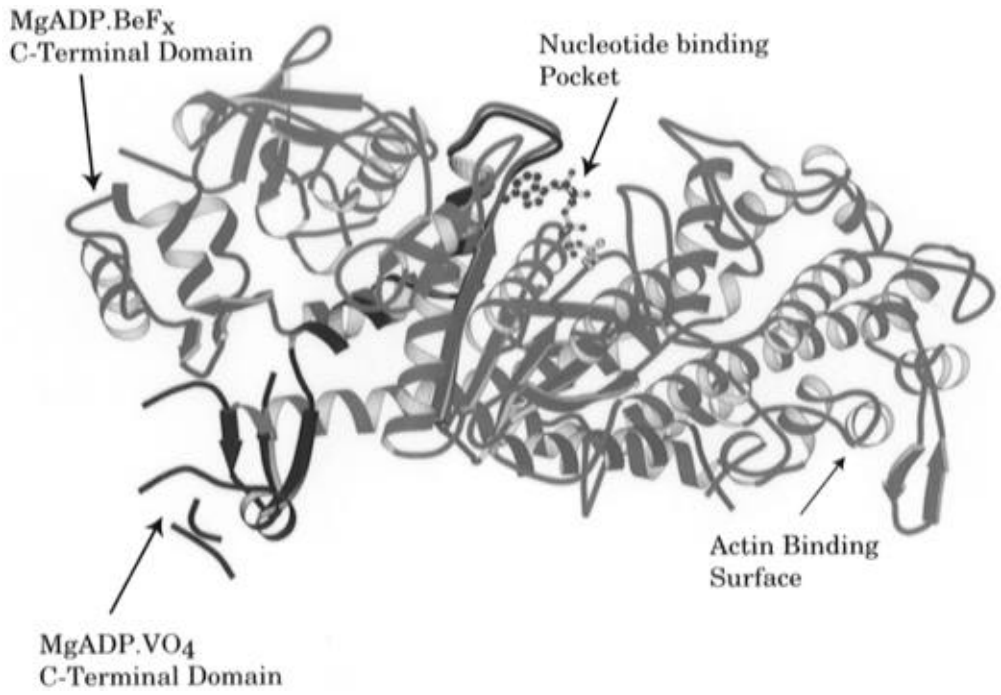

FIGURE 5: Ribbon drawing of the entire MgADP·BeF_x·S1Dc structure and residues Thr 649−Gly 749 of MgADP·VO_4·S1Dc viewed approximately parallel to the actin binding surface and looking along the nucleotide binding pocket. The structures was aligned by matching the upper domain of the central 50 kDa sections of the polypeptide chains (residues Asn 2−Gly 457) with the program LSQKAB implemented in the CCP4 program package (Kabsch, 1976; CCP4, 1994). The MgADP·BeF_x·S1Dc structure is shown in green, red, and blue to distinguish the NH_2-terminal, central, and COOH-terminal sections of the myosin heavy chain. The structure of MgADP·VO_4·S1Dc is shown in black. This reveals the dislocation of the COOH-terminal domain in S1Dc·VO_4·MgADP. This figure and Figures 6, 7, 9 and 12 were prepared with the molecular graphics program MOLSCRIPT (Kraulis, 1991).

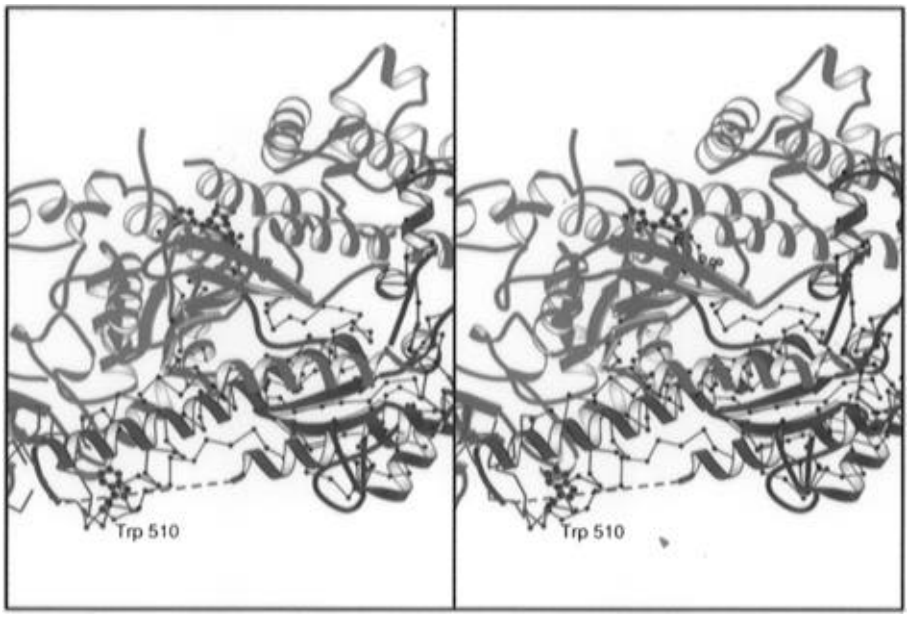

FIGURE 6: Stereoview of the changes surrounding Trp 501 in MgADP·VO_4·S1Dc relative to MgADP·BeF_x·S1Dc where the structure of the beryllium flouride complex is shown in ribbon representation with a color scheme for the heavy chain similar to that in Figure 5 with the exception that residues 454−518 are depicted in dark brown and the remainder of the lower domain of the central 50 kDa section of the heavy chain is shaded in darker red and residues Asp 518−Arg 747 in the vanadate complex are shown in α-carbon representation. Although residues Trp 501−Gly 507 are disordered in the beryllium fluoride complex, it is clear that the helix that supersedes Trp 501 has rotated approximately 24°.

fluorescence enhancement than ATP (ADP,P_i) though the latter is a mixture of states.

Conformational Changes in the 25 kDa COOH-Terminal Section. The superposition of the MgADP·BeF_x·S1Dc onto MgADP·VO_4·S1Dc, based on the least squares fit of the upper domains of the central 50 kDa section of the heavy chain (Figure 5), reveals that residues Thr 688−Gly 749 in the COOH-terminal section of the heavy chain adopt very different conformations in these structures. Indeed, relative to the position in MgADP·BeF_x·S1Dc the COOH-terminal domain in MgADP·VO_4·S1Dc has translated by more than 23 Å and rotated by approximately 70°. This change is prompted by movement of the lower domain of the 50 kDa section that in turn affects movement of the COOH-terminal

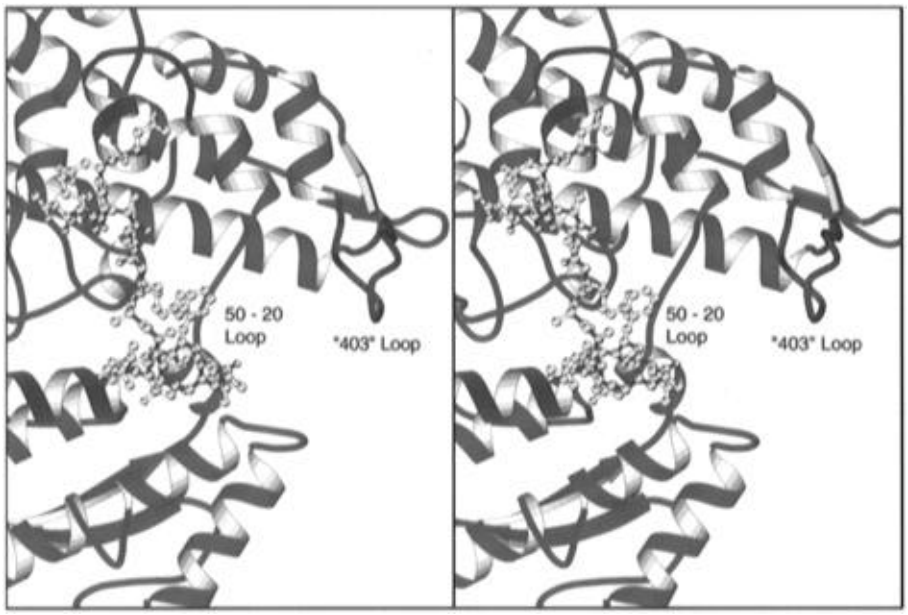

FIGURE 7: Stereoview of the junction between the 50 and 20 kDa sections of the heavy chain. All of the atoms of the variable loop are shown whereas the 50 and 20 kDa sections are depicted as ribbon representations in red and blue, respectively. The loop that contains the most common mutation in familial hypertrophic cardiomyopathy and the site of phosphorylation in some nonmuscle myosin are depicted in dark brown.

part of the molecule via the helix that connects the helix containing the reactive cysteines (Cys 697 and Cys 707) in skeletal muscle. The currently observed disposition of the COOH terminus is probably of limited biological significance due to the absence of the essential light chain. It is anticipated that this part of the molecule moves during the formation of the metastable state but that its movement is influenced by the adjacent essential light chain (Fisher et al., 1995a). This conclusion is demanded by the extensive biochemical evidence that shows that the equivalent region in skeletal muscle that encompasses the reactive cysteine residues can undergo a large conformational change when nucleotide binds (Reisler et al., 1974; Wells & Yount, 1980; Chalovich et al., 1983; Huston et al., 1988). It is well established that Cys 697 and Cys 707 can form a disulfide bond in the presence of nucleotide (Huston et al., 1988), which requires these two residues to be in close proximity. In the present structure the helix equivalent to that which separates the reactive cysteines in nucleotide-free chicken skeletal S1 is still present, which suggests that a different conformational change occurs when the essential light chain is present.

25−50 and 50−20 Loop. In all of the previous structures of myosin the loops that connect the major tryptic fragments were disordered. In the present structure weak density for the loop between the 25 and 50 kDa sections of the heavy chain could be seen but was not modeled. However, it was possible to build a single conformation for the loop that connects the central 50 kDa and COOH-terminal 20 kDa sections. This loop lies in fairly close proximity to the body of the protein and extends away from the surface only at the end close to the start of the first helix of the 20 kDa section (Figure 7). This loop has been implicated in actin binding from biochemical and model building studies (Mornet et al., 1979; Rayment et al., 1993a). The temperature factors for the loop are high and are indicative of considerable flexibility (Figure 3). It is likely that this loop adopts a different conformation when the myosin head is bound to actin. The sequence of the loop that connects the 50 and 20 kDa sections of the heavy chain is highly variable across the myosin superfamily (Warrick & Spudich, 1987; Spudich, 1994). In most cases the loops are considerably larger than observed in *Dictyostelium* myosin. There is evidence from mutagenesis of *Dictyostelium* myosin that the nature of this loop influences the kinetic parameters and motility of myosin (Uyeda et al., 1994). The present structure imposes constraints on the location of these insertions, since all myosins must recognize and bind to actin with similar binding constants.

Figure 7 also shows the orientation of the adjacent loop ("403" loop) that carries the site of phosphorylation in nonmuscle myosins (Pollard et al., 1991) and the most common mutation in familial hypertrophic cardiomyopathy (Rayment et al., 1995). This loop is believed to interact with actin (Rayment et al., 1993a). Here, the loop extends away from the surface of the protein as a short two-stranded antiparallel sheet and does not form any intermolecular contacts with symmetry-related molecules. This is in contrast to both chicken S1 and MgADP·BeF_x·S1Dc where the conformation of this loop is stabilized and influenced by interactions with neighboring molecules.

Conformation of MgADP·VO_4. The electron density for the MgADP·VO_4 is shown in Figure 8A, and the overall location of the nucleotide complex relative to the major secondary structural elements is shown in Figure 9. The conformation of ADP, the magnesium ion, and its associated water molecules is unambiguous and very similar to that seen in MgADP·BeF_x·S1Dc and MgADP·AlF_4·S1Dc. The density associated with the vanadium atom (Figure 8B) is clearly trigonal bipyramidal where three oxygen atoms lie in a plane and the axial positions are occupied by a bridging oxygen from the β-phosphate and an additional oxygen atom. The geometry of the vanadate moiety is shown in Figure 10A. The presence of a single vanadium moiety in the active site, when ADP is present, is consistent with the ^{51}V NMR studies

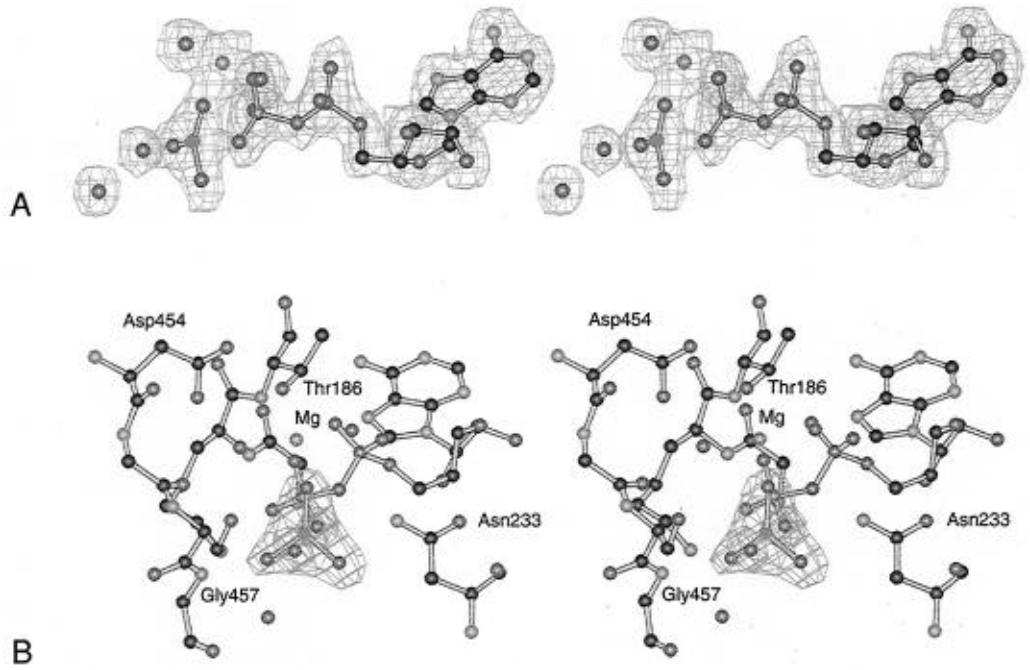

FIGURE 8: Stereoview of the electron density associated with the nucleotide binding site. (A) $2F_o - F_c$ electron density when the MgADP·vanadate complex was included in the phase calculation. (B) $F_o - F_c$ electron density when the vanadate moiety and the bridging oxygen of the β-phosphate were excluded from the refinement and phase calculation.

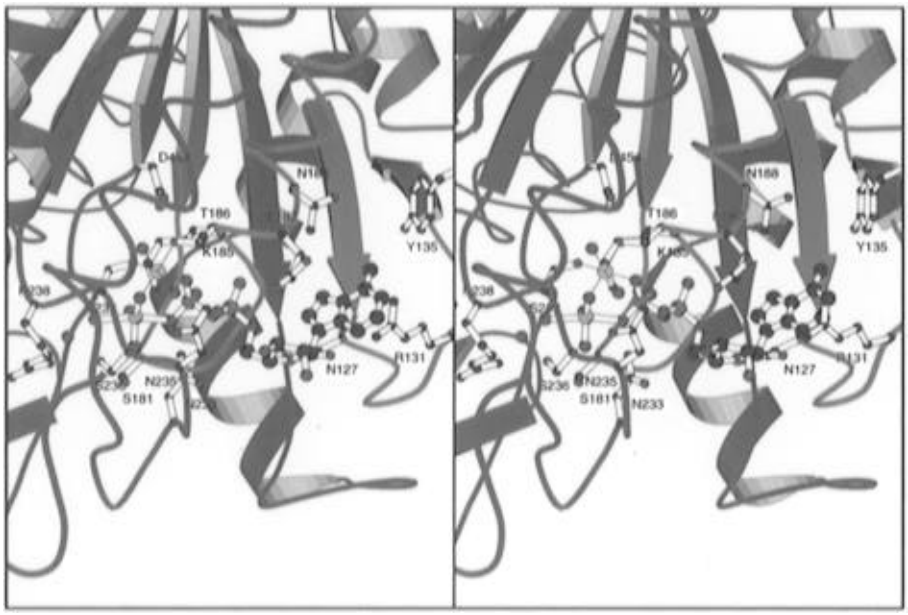

FIGURE 9: Stereo ribbon representation of the γ-phosphate pocket of MgADP·VO_4·S1Dc. The heavy chain is displayed in green, red, and blue to delineate the NH_2-terminal, central, and COOH-terminal sections that extend from residues Asp 2 to Gln 205, Gly 209 to Ala 621, and Lys 622 to Gly 749, respectively.

of the interaction between ADP, vanadate, and myosin (Ringel et al., 1990).

The vanadate moiety was refined with restraints of 90° on the apical−equatorial bond angles and with target values of 2.2 and 1.7 Å for the apical and equatorial bond distances, respectively. It is clear that the refined model fits the unrestrained electron density well. The final refined bond distances reveal that the two apical bond V−O distances are 2.3 and 2.1 Å, respectively, whereas the equatorial V−O bond distances are 1.7, 1.6, and 1.7 Å respectively. The numbering of the oxygen ligands is given in Figure 12 and Table 3. The bond distances clearly fall into two classes. Although the overall coordinate error is estimated to be ~0.2 Å, it is anticipated that the error in the active site will be less, since this is one of the better defined regions of the molecule. Thus the difference in bond length between the apical and equatorial groups is probably significant, although no distinction can be made about the bond lengths within each group. Vanadium exhibits a wide range of bond distances to oxygen ligands, where a single bond and double bond are typically 1.79 Å and typically 1.57 Å, respectively (Brown & Wu, 1976). These values suggest that the apical bonds to the vanadium ion in MgADP·VO_4·S1Dc have a valency that is considerably less than unity, whereas the equatorial bonds as a whole are greater than unity (Brown & Wu, 1976). The resolution of the X-ray data is not high enough to distinguish between a planar VO_3^- moiety with two short bonds and one long bond and a delocalized system

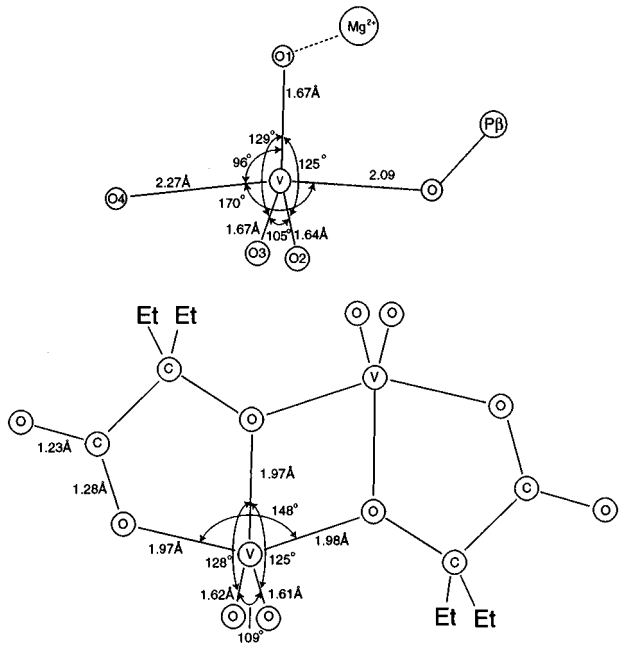

FIGURE 10: Geometry of the vanadate moiety in (A, top) the γ-phosphate binding pocket of MgADP·VO_4·S1Dc and (B, bottom) the trigonal bipyramidal vanadium complex found in $(NH_4)_2[VOC(CH_2CH_3)_2COO)(O)_2]_2$ (Hambley et al., 1992).

Table 3

		bond distances (Å)	
atom 1[a]	atom 2[a]	MgADP·VO_4	MgADP·BeF_x[b]
Thr 186 Oγ	Mg^{2+}	2.0	2.1
Ser 237 Oγ	Mg^{2+}	2.1	2.3
OW1	Mg^{2+}	2.0	2.1
OW2	Mg^{2+}	2.1	2.1
PβO1	Mg^{2+}	2.2	2.1
OV1, F1	Mg^{++}	1.9	2.1
Ser 237 N	OV1, F1	2.9	2.9 (3.0)
Ser 181 Oγ	OV2, F2	2.6	2.6 (2.9)
Ser 236 Oγ	OV2, F2	2.8	2.9 (2.8)
Asn 233 Nδ	OV2, F2	3.1	3.1 (2.9)
Lys 185 Nζ	OV3, F3	2.7	2.8 (2.9)
Gly 457 N	OV3, F3	2.8	6.9 (2.9)
Ser 236 Oγ	OV4, H_2O[c]	3.0	4.2
Ser 237 O	OV4,H_2O[c]	2.7	3.0
OW3	OV4	2.6	
OW3	Gly 457 O	2.6	
OW3	Glu 459 Oϵ2	2.7	

[a] Where there are two atoms listed, the first corresponds to an atom in MgADP·VO_4 whereas the second is the equivalent atom in MgADP·BeF_x. [b] The second entry in this column gives the distance between an atom in MgADP·BeF_x and an atom in the MgADP·VO_4·S1Dc complex after the nucleotide complex was transferred into the MgADP·VO_4·S1Dc coordinate frame. The rotation and translation matrices were derived by aligning Leu 175 to Val 187 and Asn 234 to Arg 238, the protein ligands that coordinate the nucleotides, with the program LSQKAB implemented in the CCP4 program package (Kabsch, 1976; CCP4, 1994). The nucleotides were excluded from the calculation. [c] This refers to the water molecule that is equivalent to OV4 that is coordinated to F3 in MgADP·BeF_x·S1Dc.

with three equally short bonds. However, the conformation observed in the model compounds, discussed below, favors an asymmetric arrangement.

Vanadium(V) adopts a variety of coordinations (Holloway & Melnick, 1986). The most common is a distorted octahedral coordination that contains a nonlinear VO_2^+ entity with two fairly short VO bonds (~1.64 Å) and four other ligands which show substantially longer bond distances in the range 1.9−~2.3 Å (Scheidt et al., 1971). Trigonal bipyramidal coordination with oxygen ligands is less common but has been shown to occur in solution in dimeric complexes between vanadium and 1,2-diols (Gresser & Tracey, 1986; Ray et al., 1995). The crystal structures of several model compounds including complexes with a 1,2-diol and a 2-hydroxy acid ligand have been reported (Crans et al., 1991; Hambley et al., 1992). The geometry of the latter compound, $(NH_4)_2[VOC(CH_2CH_3)_2COO)(O)_2]_2$, is shown in Figure 10B. In this complex the ligands bound to the vanadium adopt a distorted trigonal bipyramidal arrangement. The apical distances are fairly long (average 1.98 Å) whereas two of the equatorial distances are short (1.605 and 1.617 Å) and the third long (1.97 Å). Similar arrangements of ligands and bond distances have been observed in other trigonal bipyramidal complexes of vanadium(V).

Trigonal bipyramidal geometry for vanadium(V) has been observed in the active site of an enzyme in the complex of ribonuclease with uridine vanadate (Wlodawer et al., 1983) and more recently in transition-state analog complexes of rat acid phosphatase (Lindqvist et al., 1994). The latter study was at fairly low resolution such that no conclusions could be drawn about the geometry of its vanadium moiety. The structure of uridine vanadate in ribonuclease is distorted trigonal bipyramidal and similar to that seen in the model compounds (Crans et al., 1991) and in MgADP·VO_4·S1Dc even though the environment and ligands are quite different.

The protonation state of the vanadate ion in the active site when complexed with MgADP is unknown. At pH 7.0 the major monomeric species in solution is $H_2VO_4^-$ (Pope & Dale, 1968; Wells & Bagshaw, 1984). Examination of the hydrogen-bonding pattern surrounding MgADP·VO_4 (Figures 11and 12B and Table 3) suggests that the equatorial oxygen atoms coordinated to the magnesium ion (OV1) and Lys 185 (OV2) are not protonated. The third equatorial oxygen atom (OV3) is coordinated to Oγ of Ser 181, Nδ2 of Asn 233, and Oγ of Ser 236 where it appears that Ser 181 and Asn 233 both function as hydrogen donors. Oγ of Ser 236 is within hydrogen-bonding distance of both the terminal oxygen of the vanadate moiety (OV4) and the third equatorial oxygen such that its proton could be directed toward either of these atoms. Indeed, it is possible that the proton on Oγ of Ser 236 is shared by OV4 and OV2 since the angle subtended at Oγ by OV4 and OV2 is 55°. The V−O bond distance (2.3 Å) to the terminal oxygen implies this is a very weak bond and requires that this ligand is either HO^- or H_2O. Examination of the hydrogen bond network around the apical oxygen strongly suggests that OV4 is a water molecule for the following reasons. OV4 forms short hydrogen bonds to the carbonyl oxygen of Ser 237, the Oγ of Ser 236, and an additional water molecule (OW3). These ligands and vanadium ion are arranged tetrahedrally around OV4. OW3 forms additional short hydrogen bonds with good geometry to the carbonyl oxygen of Gly 457 and Oϵ2 of Glu 459. This requires that the two protons on OW3 are directed toward these latter two ligands and therefore requires a proton to reside on OV4 and be directed toward OW3. The water structure around OV4 probably plays a critical role in stabilizing the structure necessary for catalysis as discussed below.

Mechanistic Implications. It is well established that hydrolysis of ATP occurs by attack of a water molecule on the γ-phosphorus (Sleep et al., 1980; Webb & Trentham,

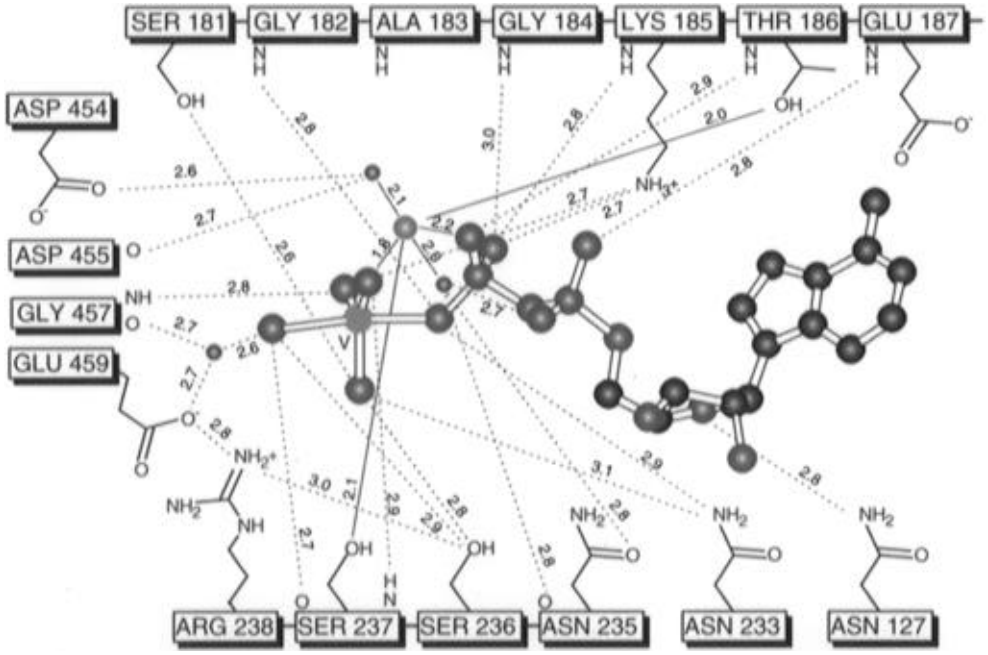

FIGURE 11: Schematic representation of the coordination of the γ-phosphate pocket in MgADP·VO_4·S1Dc. Hydrogen bonds less than 3.2 Å and ionic interactions less than 3.7 Å are shown as dashed lines with the corresponding distances. Only those interactions with the appropriate stereochemistry to participate in these interactions are included. The water molecules coordinated to the adenosine moiety and the α-phosphate have been omitted. In this figure vanadium, carbon, magnesium, nitrogen, oxygen, and phosphorus are depicted in cyan, black, orange, blue, red, and pink, respectively.

1981; Dale & Hackney, 1987); however, very little is known about the role of the protein in ATP hydrolysis. The previous studies on MgADP·BeF_x·S1Dc and MgADP·AlF_4·S1Dc suggest that contrary to earlier assumptions catalysis does not occur via a general base provided by the protein (Fisher et al., 1995a,b). Rather, it was suggested that the γ-phosphate might function as its own base and accept the proton from the nucleophilic water directly as was proposed earlier for the hydrolysis of GTP by transducin α (Sondek et al., 1994) and $p21^{ras}$ (Schweins et al., 1994, 1995). One objection to this mechanism is the poor stereochemistry for the direct transfer of the proton. To avoid this problem, an alternative mechanism was also proposed in which the Oγ of Ser 236 functions as an intermediate in the proton transfer by hydrogen exchange (Fisher et al., 1995b). Ser 236 is an absolutely conserved amino acid residue. In MgADP·VO_4·S1Dc the Oγ of Ser 236 serves as a hydrogen bond donor to both an equatorial oxygen, of the vanadate and the terminal oxygen which is consistent with Ser 236 participating in proton transfer (Fisher et al., 1995b).

As noted before, the tetrahedral beryllium fluoride adduct with MgADP mimics ATP in the active site (Fisher et al., 1995b) and represents the active site of myosin just prior to hydrolysis. In contrast, the aluminum fluoride complex is an analog of the transition state on account of the planar arrangement of fluorine ligands about the central aluminum atom and because of the longer bond between the bridging oxygen from the β-phosphate and the aluminum atom (Fisher et al., 1995b). The conformation of the protein observed in the aluminum fluoride adduct was proposed to be that necessary for hydrolysis. A detailed comparison of the hydrogen bonding in the beryllium and aluminum fluoride complexes around the γ-phosphate pocket was not discussed earlier because it was not clear how to extrapolate from the square-planar AlF_4^- ion to the trigonal bipyramidal transition state anticipated for phosphate hydrolysis. These problems are resolved by the vanadate complex such that it is possible to follow the changes that occur as a tetrahedral analog is replaced by a trigonal bipyramidal moiety in the active site. It also allows a comparison of the binding of vanadate and aluminum fluoride to myosin.

Superposition of MgADP·AlF_4·S1Dc onto MgADP·VO_4·S1Dc shows that the α- and β-phosphates adopt almost identical locations in the phosphate binding pocket (Figure 12A). The aluminum and vanadium atoms also occupy similar sites. OV3 on vanadate and F1 on AlF_4^- adopt similar positions and form an identical hydrogen bond to the amide hydrogen on Gly 457. This reveals that the square planar AlF_4^- ion is accommodated in the active site by plasticity in the hydrogen bonding to the other ligands in the γ-phosphate pocket. F4 forms an ionic interaction with the magnesium ion even though it lies in a different position from the corresponding oxygen ligand in the vanadate complex. F2 and F3 fulfill many of the interactions formed by OV2 in the vanadate complex such that the extra ligand provided by AlF_4^- compared to VO_3^- is accommodated around OV2. In order to maintain octahedral geometry around the magnesium ion, the other ligands to the metal undergo compensatory movements. In particular, Oγ of Ser 237 moves by 0.9 Å, which allows the formation of a hydrogen bond between Oγ of Ser 237 and F2 (2.9 Å) that is not observed in the vanadate complex. An additional interaction is also seen between F2 and the amide hydrogen on Ser 237. The one water molecule coordinated to the magnesium ion that was clearly defined in the aluminum fluoride complex also moves by 0.6 Å.

Overlay of ADP·BeF_x onto the active site of MgADP·VO_4·S1Dc (Figure 12B) reveals that the α- and β-phosphates and ribose of these complexes adopt almost identical locations in the phosphate binding pocket. The hydrogen bond distances to the coordinating ligands of VO_4 and BeF_x in their respective structures and in the superimposed

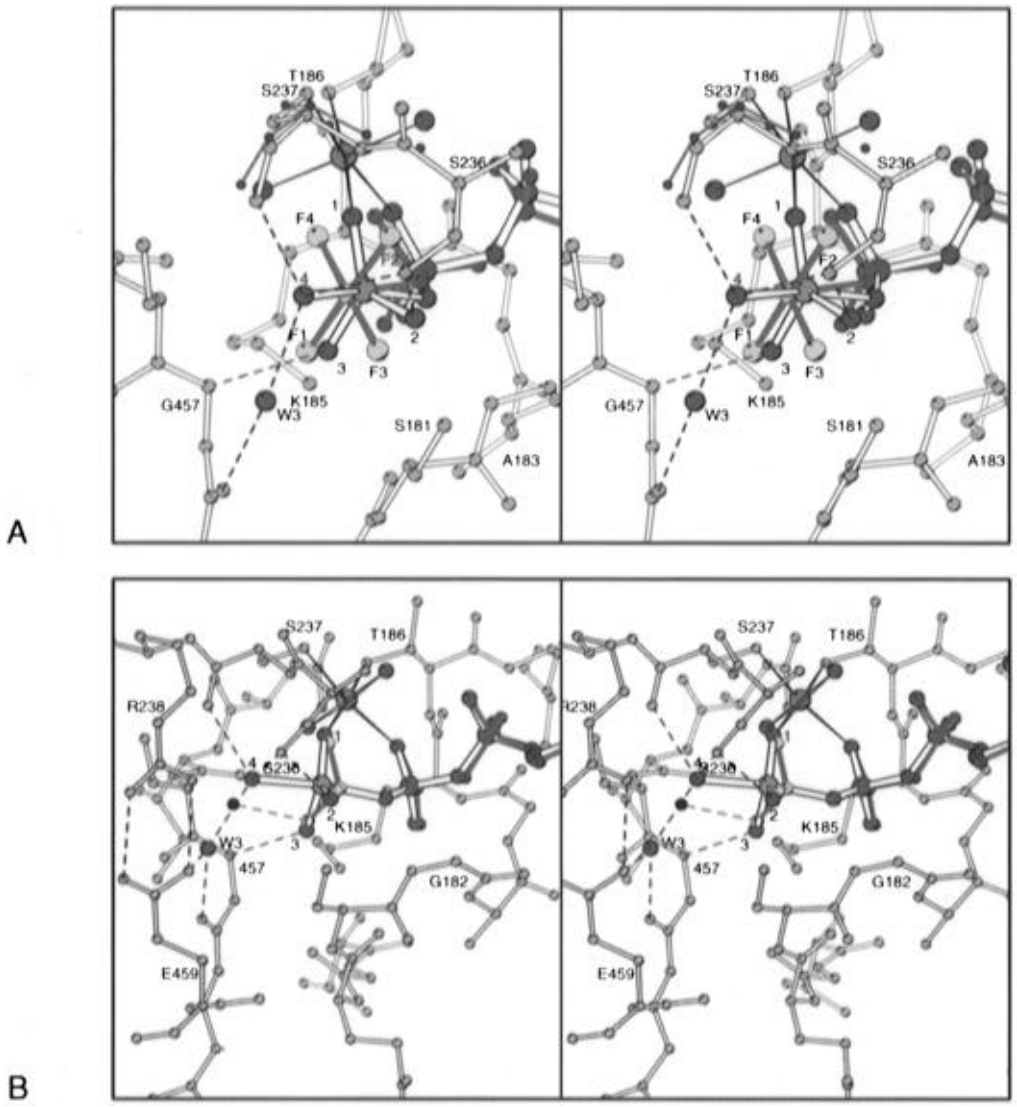

FIGURE 12: A close-up stereoview of the γ-phosphate binding pocket of MgADP·VO_4·S1Dc onto which (A) ADP·AlF_4 and b) ADP·BeF_x have been superimposed. The rotation and translation matrices were derived by aligning the protein ligands that coordinate the nucleotide (Leu 175−Val 187, Asn 234−Arg 238, and Asp 454−Asp 459 for MgADP·ALF_4 and Leu 175−Val 187 and Asn 234−Arg 238 for Mg·ADP·BeF_x) with the program LSQKAB implemented in the CCP4 program package (Kabsch, 1976; CCP4, 1994) (rms differences of 0.37 and 0.38 Å, respectively). The nucleotides were excluded from the calculations. The magnesium ion, its associated water molecules, and the protein atoms are shown for MgADP·VO_4·S1Dc. Ser 236 and one of the water molecules bound to the magnesium ion in MgADP·AlF_4·S1Dc are also shown in dark gray. For clarity, the other atoms in MgADP·AlF_4·S1Dc and MgADP·BeF_x·S1Dc are not shown since their positions are not significantly different from those of the vanadate complex.

structure are given in Table 3. This suggests that the leaving group, MgADP, does not change significantly as the transition state is approached (at least within the experimental error of these structures). The overlap also shows that the three fluorine ligands of BeF_x and three equatorial ligands on vanadate lie close to the same plane. Furthermore, the rotational orientation of each set of three atoms is very similar in both complexes. This suggests (if BeF_x and VO_4 are assumed to be models of the ground and transition states) that in going from the ATP ground state to the transition state the oxygen atoms remain close to the observed position of the fluorines and vanadium oxygens while the phosphorus to oxygen distance increases. This fits into the expected picture for phosphate hydrolysis. However, Figure 12B poses an interesting question of why the BeF_x adduct does not adopt the conformation observed in the vanadate complex? On the basis of the earlier structure of the aluminum fluoride complex it was suggested that the transition-state conformation was attained because the longer Al−O bond distance allowed the formation of the additional hydrogen bond to the amide hydrogen of Gly 457 (Fisher et al., 1995b). However, a fluorine atom of BeF_x is only 2.9 Å from the amide nitrogen of Gly 457 when transferred to the vanadate active site. This is not significantly different from the observed hydrogen bond distance of 2.8 Å between OV3 and this amide nitrogen in the vanadate complex. If the hydrogen bond distances alone are indicative of strength, why does the polypeptide chain in the MgADP·BeF_x·S1Dc complex adopt a different conformation from that seen in MgADP·VO_4·S1Dc? The alternative question is what are the factors that stabilize the conformation of the MgADP·VO_4·S1Dc complex? These are difficult questions to answer. One possible difference between these two arrangements lies in the orientation of the hydrogen bond acceptor atoms of the vanadate and BeF_x and the orientation of the amide hydrogen. The V−Ô−N and Be−F̂−N bond angles are 131° and 160°, respectively, whereas the amide hydrogen is estimated to be in direct line with the vanadate oxygen.

However, there is little relationship between the length (and strength) and the angle at the acceptor group, although angles for most hydrogen bonds cluster about 129° in proteins where the hydrogen bond is not restricted by secondary structural constraints (Baker & Hubbard, 1984). A more likely reason for differences in conformation adopted by the BeF_x and vanadate complexes is the differences in the water structure surrounding these moieties in the γ-phosphate pocket.

There is an extensive hydrogen bond network surrounding the apical oxygen (or water) of the vanadate moiety with an approximately tetrahedral distribution of ligands. This suggests that the axial approach of the nucleophilic water molecule on the γ-phosphorus of ATP would be stabilized by these interactions. The constellation of interactions that stabilizes the location of the water molecule in the vanadate complex is not available in the beryllium fluoride complex. The equivalent water molecule in MgADP·BeF_x·S1Dc is hydrogen bonded to F3 and the carbonyl oxygen of Ser 237, where the protons on the water molecule are oriented toward these two hydrogen bond acceptors (Figure 12B). It lies approximately 1.1 Å from the location of the apical water (OV4) on the vanadate moiety in MgADP·VO_4·S1Dc. In order for the protein to adopt the conformation observed in MgADP·VO_4·S1Dc, the water molecule associated with F3 must move; otherwise, it will experience a bad contact with the α-carbon of Ser 456. Likewise, if this water is to undergo nucleophilic attack on the terminal phosphorus, it must move to an in-line position, similar to that occupied by OV4 in the vanadate moiety. However, movement of the water molecule to an in-line location, in the absence of a conformational change in the protein, would be unfavorable for two reasons. It would lack the conformational stability provided by OW3 (whose location is also a consequence of the conformational change) and also lose its earlier hydrogen bond to F3. Furthermore, once in the in-line position the water molecule could not form reasonable hydrogen bonds with any of the other fluorine atoms. The latter arises not only from geometric considerations but also because movement into the in-line position requires that the protons on the attacking water be directed away from the fluorine atoms to form hydrogen bonds with Oγ of Ser 236 and OW3. Thus it would appear that the conformation observed in MgADP·VO_4·S1Dc is optimized to orient a water molecule for nucleophilic attack on the γ-phosphorus atom. Conversely, this suggests that premature hydrolysis of ATP and loss of hydrolysis products when the apex of the γ-phosphate pocket is open is prevented by the stereochemically restricted environment of the active site.

There has been considerable discussion over the nature of the transition state for phosphoryl transfer in enzymes and in solution (Westheimer, 1987). In reactions with model compounds in aqueous solution there is compelling evidence for a metaphosphate-like transition state which is essentially dissociative without the formation of metaphosphate itself [see Herschlag and Jencks (1989) and references cited therein]. The situation is less clear for enzymatically catalyzed reactions, many of which involve participation of a divalent cation in the nucleotide binding (Hollfelder & Herschlag, 1995). It has been shown in solution that divalent cations such as Mg^{2+} do not increase the associative character of the transition state (Herschlag & Jencks, 1987). However, the experiments on model compounds have not necessarily emulated the environment of the active site of an enzyme. In particular, it is difficult to simulate the restricted stereochemistry and ionic configuration provided by a nucleotide binding site. The structure of MgADP·VO_4·S1Dc provides a glimpse of the environment that is likely to surround a metaphosphate-like intermediate at the transition state. Unfortunately, in the absence of additional spectral studies, it is impossible to correlate the structure of the vanadium in the active site with the bond order at the transition state for myosin. Such a study has been carried out and described in great detail for muscle phosphoglucomutase by Ray and coworkers (Ray et al., 1990; Ray & Post, 1990; Deng et al., 1993; Ray et al., 1993) from which it was concluded that there is significant bond order to the attacking and leaving groups in the transition state for phosphoryl transfer in this enzyme. For myosin it would appear that there is no difference in the environment or structure of the ligands that coordinate ADP in either MgADP·BeF_x·S1Dc and MgADP·VO_4·S1Dc. This suggests that the leaving group (ADP) experiences a very similar environment in the ground and transition states. Rather it seems that hydrolysis requires a conformational change in the protein that orients the nucleophilic water for attack on the γ-phosphate. This structure appears to be more consistent with greater bond order to the attacking and leaving groups in the transition state for hydrolysis than anticipated for a purely dissociative mechanism.

Finally, it is of interest that formation of the ternary complex between vanadate, MgADP, and myosin is many orders of magnitude slower than would be expected from a diffusion-limited reaction. This was previously interpreted as evidence for a slow conformational change in the protein following the initial binding of vanadate (Goodno, 1979). The structural change observed between MgADP·BeF_x·S1Dc and MgADP·VO_4·S1Dc could be viewed as consistent with those observations. However, the onset of inhibition by beryllium fluoride is also slow, even though this complex exhibits the same conformation as that seen in $MgPP_i$·S1Dc (Smith & Rayment, 1995). Thus is seems likely that the slow inhibition is a more complex process associated with formation of a ternary chemical species in the active site.

CONCLUSION

In recent years vanadate has been often replaced by aluminum and beryllium fluoride as a phosphate analog in biochemical studies (Chabre, 1990) on account of vanadate's tendency to polymerize at physiological hydrogen ion concentrations (Pope & Dale, 1968) and because it is photoreactive (Gibbons et al., 1987; Grammer et al., 1988). Indeed, aluminum and beryllium fluoride bind and affect the properties of a wide range of enzymes that includes the G-proteins (Sternweis & Gilman, 1982; Bigay et al., 1985, 1987), actin and tubulin (Combeau & Carlier, 1988, 1989), and myosin (Phan & Reisler, 1992; Werber et al., 1992; Maruta et al., 1993; Phan et al., 1993). However, neither of these metallofluorides functions as a true analog of the transition state for phosphate ester bond cleavage. In myosin, the beryllium fluoride moiety observed in the active site is tetrahedral such that the complex with ADP mimics ATP and is more representative of the ground state prior to hydrolysis (Fisher et al., 1995b). Conversely, aluminum fluoride forms a complex with the corresponding nucleotide diphosphate in both the G-proteins and myosin where the coordination of the aluminum is approximately square

bipyramidal (Coleman et al., 1994; Sondek et al., 1994; Fisher et al., 1995b). The aluminum fluoride complex is believed to mimic the transition state for hydrolysis, at least insofar as the biological properties of the protein are concerned; however, the extra fluorine ligand prevents it from being a true analog. The structure of MgADP·VO_4·S1Dc described here shows how the extra fluorine ligand is accommodated in myosin's active site and demonstrates again that vanadate is a good structural analog of the transition state for phosphoryl transfer.

ACKNOWLEDGMENT

We thank Ralph Yount (Washington State University) for providing the ATP affinity column to purify S1Dc and for helpful suggestions, Robert Smith for preparing the protein used in this investigation, J. B. Thoden, M. M. Benning, and J. E. Wedekind for help with data collection, G. Wesenberg for computational analysis, and A. J. Fisher, A. M. Gulick, P. A. Frey, G. H. Reed, and W. W. Cleland (University of Wisconsin) and E. Taylor (University of Chicago) for helpful discussions. Help from Hazel M. Holden in completing the crystallographic refinement is also gratefully acknowledged.

REFERENCES

Arndt, U. W., & Wonacott, A. J. (1977) *The Rotation Method in Crystallography*, North-Holland, Amsterdam.
Bagshaw, C. R., & Trentham, D. R. (1973) *Biochem. J. 133*, 323−328.
Bagshaw, C. R., & Trentham, D. R. (1974) *Biochem. J. 141*, 331−349.
Baker, E. N., & Hubbard, R. E. (1984) *Prog. Biophys. Mol. Biol. 44*, 97−179.
Bigay, J., Deterre, P., Pfister, C., & Chabre, M. (1985) *FEBS Lett. 191*, 181−185.
Bigay, J., Deterre, P., Pfister, C., & Chabre, M. (1987) *EMBO J. 6*, 2907−2913.
Bivin, D. B., Kubota, S., Pearlstein, R., & Morales, M. F. (1993) *Proc. Natl. Acad. Sci. U.S.A. 90*, 6791−6795.
Brown, I. D., & Wu, K. K. (1976) *Acta Crystallogr. B32*, 1957−1959.
Brünger, A. T. (1990) *X-PLOR Version 3.1: A System for Crystallography and NMR*, Yale University, New Haven, CT.
Brünger, A. T., Kuriyan, J., & Karplus, M. (1987) *Science 235*, 458−460.
CCP4 (1994) *Acta Crystallogr. D50*, 760−763.
Chabre, M. (1990) *Trends Biochem. Sci. 15*, 6−10.
Chalovich, J. M., Greene, L. E., & Eisenberg, E. (1983) *Proc. Natl. Acad. Sci. U.S.A. 80*, 4909−4913.
Chase, P. B., Martyn, D. A., Kushmerick, M. J., & Gordon, A. M. (1993) *J. Physiol. 460*, 231−246.
Coleman, D. E., Berghuis, A. M., Lee, E., Linder, M. E., Gilman, A. G., & Sprang, S. R. (1994) *Science 265*, 1405−1412.
Combeau, C., & Carlier, M.-F. (1988) *J. Biol. Chem. 263*, 17429−17436.
Combeau, C., & Carlier, M.-F. (1989) *J. Biol. Chem. 264*, 19017−19021.
Crans, D. C., Felty, R. A., & Miller, M. M. (1991) *J. Am. Chem. Soc. 113*, 265−269.
Cremo, C. R., Grammer, J. C., & Yount, R. G. (1988) *Biochemistry 27*, 8415−8420.
Cremo, C. R., Grammer, J. C., & Yount, R. G. (1989) *J. Biol. Chem. 264*, 6608−6611.
Dale, M. P., & Hackney, D. D. (1987) *Biochemistry 26*, 8365−8372.
Dantzig, J. A., & Goldman, Y. E. (1985) *J. Gen. Physiol. 86*, 305−327.
Deng, H., Ray, W. J., Jr., Burgner, J. W., II, & Callender, R. (1993) *Biochemistry 32*, 12984−12992.
Fisher, A. J., Smith, C. A., Thoden, J., Smith, R., Sutoh, K., Holden, H. M., & Rayment, I. (1995a) *Biophys. J. 68*, 19s−28s.
Fisher, A. J., Smith, C. A., Thoden, J., Smith, R., Sutoh, K., Holden, H. M., & Rayment, I. (1995b) *Biochemistry 34*, 8960−8972.
Gibbons, I. R., Lee-Eiford, A., Mocz, G., Phillipson, C. A., Tang, W.-J. Y., & Gibbons, B. H. (1987) *J. Biol. Chem. 262*, 2780−2786.
Goldman, Y. E. (1987) *Annu. Rev. Physiol. 49*, 637−654.
Goodno, C. C. (1979) *Proc. Natl. Acad. Sci. U.S.A. 76*, 2620−2624.
Goodno, C. C. (1982) in *Methods in Enzymology* (Frederiksen, D., & Cunningham, L., Eds.) pp 116−123, Academic Press, New York.
Goodno, C. C., & Taylor, E. W. (1982) *Proc. Natl. Acad. Sci. U.S.A. 79*, 21−25.
Grammer, J. C., Cremo, C. R., & Yount, R. G. (1988) *Biochemistry 27*, 8408−8415.
Gresser, M. J., & Tracey, A. S. (1986) *J. Am. Chem. Soc. 108*, 1935−1939.
Gresser, M. J., & Tracey, A. S. (1990) in *Vanadium in Biological Systems: Physiology and Biology* (Chasteen, D. N., Ed.) pp 63−80, Kluwer, Amsterdam, The Netherlands.
Hambley, T. W., Judd, R. J., & Lay, P. A. (1992) *Inorg. Chem. 31*, 343−345.
Henry, G. D., Maruta, S., Ikebe, M., & Sykes, B. D. (1993) *Biochemistry 32*, 10451−10456.
Herschlag, D., & Jencks, W. P. (1987) *J. Am. Chem. Soc. 109*, 4665−4674.
Herschlag, D., & Jencks, W. P. (1989) *J. Am. Chem. Soc. 111*, 7579−7586.
Hiratsuka, T. (1992) *J. Biol. Chem. 267*, 14949−14954.
Hollfelder, F., & Herschlag, D. (1995) *Biochemistry 34*, 12255−12264.
Holloway, C. E., & Melnick, M. (1986) *Rev. Inorg. Chem. 8*, 288−361.
Huston, E. E., Grammer, J. C., & Yount, R. G. (1988) *Biochemistry 27*, 8945−8952.
Johnson, W. C., Bivin, D. B., Ue, K., & Morales, M. F. (1991) *Proc. Natl. Acad. Sci. U.S.A. 88*, 9748−9750.
Jones, T. A. (1978) *J. Appl. Crystallogr. 11*, 268−272.
Jones, T. A. (1985) in *Methods in Enzymology* (Wycoff, H. W., Hirs, C. H. W., & Timasheff, S. N., Eds.) pp 157−171, Academic Press Inc., New York.
Jones, T. A., Zou, J.-Y., Cowan, S. W., & Kjeldgaard, M. (1991) *Acta Crystallogr. A47*, 110−119.
Kabsch, W. (1976) *Acta Crystallogr. A32*, 922−923.
Kraulis, P. J. (1991) *J. Appl. Crystallogr. 24*, 946−950.
Lindquist, R. N., Lynn, J. L. J., & Lienhard, G. E. (1973) *J. Am. Chem. Soc. 95*, 8762−8768.
Lindqvist, Y., Schneider, G., & Vihko, P. (1994) *Eur. J. Biochem. 221*, 139−142.
Luzzati, V. (1952) *Acta Crystallogr. 5*, 802−810.
Lymn, R. W., & Taylor, E. W. (1971) *Biochemistry 10*, 4617−4624.
Maruta, S., Henry, G. D., Sykes, B. D., & Ikebe, M. (1993) *J. Biol. Chem. 268*, 7093−7100.
Morita, F. (1967) *J. Biol. Chem. 242*, 4501−4506.
Mornet, D., Pantel, P., Audemard, E., & Kassab, R. (1979) *Biochem. Biophys. Res. Commun. 89*, 925−932.
Navaza, J. (1993) *Acta Crystallogr. D49*, 588−591.
Otwinowski, Z. (1986) Ph.D. Thesis, Yale University, New Haven, CT.
Papp, S. J., & Highsmith, S. (1993) *Biochim. Biophys. Acta 1202*, 169−172.
Phan, B., & Reisler, E. (1992) *Biochemistry 31*, 4787−4793.
Phan, B. C., Faller, L. D., & Reisler, E. (1993) *Biochemistry 32*, 7712−7719.
Pollard, T. D., Doberstein, S. K., & Zot, H. G. (1991) *Annu. Rev. Physiol. 53*, 653−681.
Pope, M. T., & Dale, B. W. (1968) *Q. Rev. Chem. Soc. 22*, 527−548.
Ramakrishnan, C., & Ramachandran, G. N. (1965) *Biophys. J. 5*, 909−933.
Ray, W. J., Jr., & Post, C. B. (1990) *Biochemistry 29*, 2779−2789.
Ray, W. J., Jr., Burgner, J. W., II, & Post, C. B. (1990) *Biochemistry 29*, 2770−2778.
Ray, W. J., Jr., Burgner, J. W., II, Deng, H., & Callender, R. (1993) *Biochemistry 32*, 12977−12983.

Ray, W. J., Crans, D. C., Zheng, J., Burgner, J. W., Deng, H., & Mahroof-Tahir, M. (1995) *J. Am. Chem. Soc. 117*, 6015−6026.
Rayment, I., Holden, H. M., Whittaker, M., Yohn, C. B., Lorenz, M., Holmes, K. C., & Milligan, R. A. (1993a) *Science 261*, 58−65.
Rayment, I., Rypniewski, W. R., Schmidt-Bäse, K., Smith, R., Tomchick, D. R., Benning, M. M., Winkelmann, D. A., Wesenberg, G., & Holden, H. M. (1993b) *Science 261*, 50−58.
Rayment, I., Holden, H. M., Sellers, J. R., Fananapazir, L., & Epstein, N. D. (1995) *Proc. Natl. Acad. Sci. U.S.A. 92*, 3864−3868.
Rayment, I., Smith, C. A., & Yount, R. G. (1996) *Annu. Rev. Physiol. 58*, 671−702.
Read, R. J. (1986) *Acta Crystallogr. A42*, 140−149.
Reisler, E., Burke, M., Himmelfarb, S., & Harrington, W. F. (1974) *Biochemistry 13*, 3837−3840.
Ringel, I., Peyser, Y. M., & Muhlrad, A. (1990) *Biochemistry 29*, 9091−9096.
Ritchie, M. D., Geeves, M. A., Woodward, S. K. A., & Manstein, D. J. (1993) *Proc. Natl. Acad. Sci. U.S.A. 90*, 8619−8623.
Rodgers, D. W. (1994) *Structure 2*, 1135−1140.
Scheidt, W. R., Tsai, C.-C., & Hoard, J. L. (1971) *J. Am. Chem. Soc. 93*, 3867−3872.
Schweins, T., Langen, R., & Warshel, A. (1994) *Nat. Struct. Biol. 1*, 476−484.
Schweins, T., Geyer, M., Scheffzek, K., Warshel, A., Kalbitzer, H. R., & Wittinghofer, A. (1995) *Struct. Biol. 2*, 36−44.
Sleep, J. A., Hackney, D. D., & Boyer, P. D. (1980) *J. Biol. Chem. 255*, 4094−4099.
Smith, C. A., & Rayment, I. (1995) *Biochemistry 34*, 8973−8981.
Smith, S. J., & Eisenberg, E. (1990) *Eur. J. Biochem. 193*, 69−73.
Smith, T. J. (1993) *J. Appl. Crystallogr. 26*, 496−498.
Sondek, J., Lambright, D. G., Noel, J. P., Hamm, H. E., & Sigler, P. B. (1994) *Nature 372*, 276−279.
Spudich, J. A. (1994) *Nature 372*, 515−518.
Sternweis, P. C., & Gilman, A. G. (1982) *Proc. Natl. Acad. Sci. U.S.A. 79*, 4888−4891.
Taylor, E. W. (1977) *Biochemistry 16*, 732−740.
Teng, T. Y. (1990) *J. Appl. Crystallogr. 23*, 387−391.
Trentham, D. R., Eccleston, J. F., & Bagshaw, C. R. (1976) *Q. Rev. Biophys. 9*, 217−281.
Tronrud, D. E., Ten Eyck, L. F., & Matthews, B. W. (1987) *Acta Crystallogr. A43*, 489−501.
Trybus, K. M., & Taylor, E. W. (1982) *Biochemistry 21*, 1284−1294.
Uyeda, T. Q. P., Ruppel, K. M., & Spudich, J. A. (1994) *Nature 368*, 567−569.
Warrick, H. M., & Spudich, J. A. (1987) *Annu. Rev. Cell Biol. 3*, 379−421.
Webb, M. R., & Trentham, D. R. (1981) *J. Biol. Chem. 256*, 10910−10916.
Wells, C., & Bagshaw, C. R. (1984) *J. Muscle Res. Cell Motil. 5*, 97−112.
Wells, J. A., & Yount, R. G. (1980) *Biochemistry 19*, 1711−1717.
Werber, M. M., Szent-Gyorgyi, A. G., & Fasman, G. D. (1972) *Biochemistry 11*, 2872−2883.
Werber, M. M., Peyser, Y. M., & Muhlrad, A. (1987) *Biochemistry 26*, 2903−2909.
Werber, M. M., Peyser, M., & Muhlrad, A. (1992) *Biochemistry 31*, 7190−7197.
Westheimer, F. H. (1987) *Science 235*, 1173−1178.
Wilson, G. J., Shull, S. E., & Cooke, R. (1995) *Biophys. J. 68*, 216−226.
Wlodawer, A., Miller, M., & Sjolin, L. (1983) *Proc. Natl. Acad. Sci. U.S.A. 80*, 3628−3631.
Yount, R. G., Cremo, C. R., Grammer, J. C., & Kerwin, B. A. (1992) *Philos. Trans. R. Soc. London B336*, 55−61.

BI952633+